
PIPEFUSION: PATCH-LEVEL PIPELINE PARALLELISM FOR DIFFUSION TRANSFORMERS INFERENCE

Jiarui Fang^{*1} JinZhe Pan^{*12} Jiannan Wang^{*13} Aoyu Li¹ Xibo Sun¹

ABSTRACT

This paper presents PipeFusion, an innovative parallel methodology to tackle the high latency issues associated with generating high-resolution images using diffusion transformers (DiTs) models. PipeFusion partitions images into patches and the model layers across multiple GPUs. It employs a patch-level pipeline parallel strategy to orchestrate communication and computation efficiently. By capitalizing on the high similarity between inputs from successive diffusion steps, PipeFusion reuses one-step stale feature maps to provide context for the current pipeline step. This approach notably reduces communication costs compared to existing DiTs inference parallelism, including tensor parallel, sequence parallel and DistriFusion. PipeFusion also exhibits superior memory efficiency, because it can distribute model parameters across multiple devices, making it more suitable for DiTs with large parameter sizes, such as Flux.1. Experimental results demonstrate that PipeFusion achieves state-of-the-art performance on 8×L40 PCIe GPUs for Pixart, Stable-Diffusion 3 and Flux.1 models. Our Source code is available at <https://github.com/xdit-project/xdit>.

1 INTRODUCTION

In recent years, the capabilities of AI-generated content (AIGC) have rapidly advanced, with diffusion models emerging as a leading generative technique in image (BlackForestLabs, 2024; Esser et al., 2024; Chen et al., 2024a; Peebles & Xie, 2023) and video synthesis (OpenAI, 2024; MetaAI, 2024). The model architecture of diffusion models is undergoing a significant transformation. Traditionally dominated by U-Net (Ronneberger et al., 2015) architectures, these models are now transitioning to Diffusion Transformers (DiTs) (Peebles & Xie, 2023). The context length of diffusion models is also increasing, which is crucial for handling long videos and high-resolution images. For example, the current leading open-source image generation model, Flux.1 (BlackForestLabs, 2024), generates images with a resolution of 1024px (1024x1024), requiring a sequence length of 262 thousand tokens; For 4096px resolution images, the input sequence increases to 4.2 million tokens.

The inference latency of generating long visual sequences from DiTs models is notably high due to the quadratic growth in computation time with the sequence length because of the attention mechanism. Given that a single GPU cannot satisfy the latency requirements for practical applications, it becomes necessary to parallelize the DiTs inference

for a single image across multiple computational devices. However, tensor parallelism (TP) (Shoeybi et al., 2019) commonly used in serving Large Language Models (LLMs) is inefficient for DiTs due to their large activation volumes. In such cases, the communication costs often outweigh the benefits of parallel computation. To address the challenges posed by long sequences, sequence parallelism (SP) (Jacobs et al., 2023; Liu et al., 2023) is applied for the parallel inference of DiTs, which partitions the input image into patches and needs data exchange across different devices in the attention operations.

DiTs inference features *input temporal redundancy* (So et al., 2023; Ma et al., 2024b;a; Yuan et al., 2024; Zhao et al., 2024; MetaAI, 2024), indicating a high degree of similarity in both inputs and activations across successive diffusion time steps, which can be leveraged to design more efficient parallel approaches. DistriFusion (Li et al., 2024) is a sequence parallelism approach that capitalizes on this characteristic applied for U-Net-based diffusion models. By utilizing local fresh activations in conjunction with stale activations from the previous step, DistriFusion engages in attention and convolution operations. This technique effectively overlaps communication costs within the computation of a diffusion timestep. However, when this method is applied to DiTs, it has a significant drawback of excessive memory usage. DistriFusion maintains the full spatial shape of attention keys (K) and values (V) for all layers. Its memory cost is directly proportional to the sequence length.

We discovered that the potential for DiTs-specific paral-

^{*}Equal contribution ¹Tencent ²Huazhong University of Science and Technology ³The University of Hong Kong. Correspondence to: Jiarui Fang <fangjiarui123@gmail.com>.

lelism leveraging input temporal redundancy has not been fully exploited. Existing parallel paradigms, whether TP or SP, require communication of Activations for each DiTs block. In contrast, sequence-level parallel methods like TeraPipe (Li et al., 2021), which only need to transfer limited input activations, have not been sufficiently explored. However, TeraPipe is tailored for training LLMs and operates on the assumption that the model uses causal attention. This means that each input token only attends to tokens that come before it. However, DiTs utilize full attention, where each token must attend to all tokens that precede and follow it. Therefore, a direct application of sequence-level pipeline parallelism is not feasible in DiTs. To address this challenge, our paper introduces an innovative approach named **PipeFusion** that strategically harnesses Input Temporal Redundancy to develop an efficient patch-level pipeline parallelism suitable for DiTs parallel inference. Similar to DistriFusion, when the current pipeline step does not have access to the most recent K and V values, it employs the stable K and V from the previous step, which are approximate to the current ones. This approach allows for more efficient parallel processing in DiTs, capitalizing on the inherent redundancy in input sequences.

PipeFusion demonstrates advantages in communication costs, memory usage, and generation accuracy. Firstly, compared to existing DiTs parallel methods, PipeFusion substantially reduces inter-device communication costs. It only transfers the input of the initial layer and the output of the final layer on each device, whereas other parallel approaches, i.e. sequence and tensor parallel, require to transmit activations for every DiT layer. Secondly, PipeFusion offers lower memory consumption by distributing model parameters across multiple devices. This makes it particularly suitable for DiTs with large model parameters, such as the 12B Flux model (BlackForestLabs, 2024). In contrast to DistriFusion, PipeFusion reduces the memory buffers required for attention K, V to $1/N$ (N is the parallel degree). Finally, PipeFusion, by utilizing fresh K and V values over a longer period, achieves higher image generation accuracy compared to DistriFusion, thus being closer to the serial inference results. Experimental results show that PipeFusion achieves the lowest DiTs inference latency on $8 \times L40$ PCIe-connected GPUs compared to sequence parallelism, DistriFusion, and tensor parallelism.

Our contributions are as follows:

- We systematically investigated the parallel approaches applicable to DiTs, including Tensor Parallel (TP), and Sequence Parallel (SP). We also adapted an asynchronous SP variant DistriFusion from U-Net-based models to DiTs.
- We proposed a Patch-level Pipeline Parallel method,

PipeFusion, which perfectly combines Input Temporal Redundancy with the TeraPipe. This method achieves the lowest communication cost and reduces the memory consumption of model parameters.

- On the latest DiTs—Pixart, Stable Diffusion 3, and Flux.1—PipeFusion demonstrated significant advantages in both inference latency and memory usage.

2 BACKGROUND & RELATED WORKS

Diffusion Models: Diffusion models utilize a noise-prediction deep neural network (DNN) denoted by ϵ_θ to generate a high-quality image. The process starts from pure Gaussian noise $x_T \sim \mathcal{N}(0, I)$ and involves numerous iterative denoising steps to produce the final meaningful image x_0 , with T representing the total number of diffusion time steps. As shown in Figure 1, at each diffusion time step t , given the noisy image x_t , the model ϵ_θ takes x_t , t , and an additional condition c (e.g., text, image) as inputs to predict the corresponding noise ϵ_t within x_t . At each denoising step, the previous image x_{t-1} can be obtained from the following equation:

$$x_{t-1} = \text{Update}(x_t, t, \epsilon_t), \quad \epsilon_t = \epsilon_\theta(x_t, t, c). \quad (1)$$

In this context, Update denotes a function that is specific to the sampler, i.e. DDIM (Song et al., 2020) and DPM (Lu et al., 2022), generally involves operations such as element-wise operations. After multiple steps, we decode x_0 from the Latent Space to the Pixel Space using a Variational Autoencoder (VAE) (Kingma & Welling, 2013). Consequently, the predominant contributor to diffusion model inference latency is attributed to the forward propagation through the model ϵ_θ .

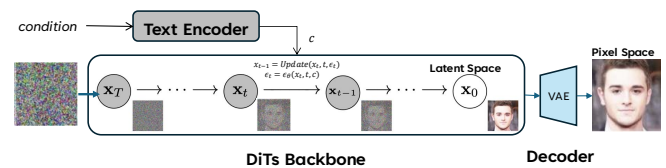


Figure 1. Workflow of DiTs inference.

Diffusion Transformers (DiTs): The architecture of diffusion model ϵ_θ is undergoing a pivotal transition from U-Net (Ronneberger et al., 2015) to Diffusion Transformers (DiTs) (Jiang et al., 2024; Chen et al., 2023; Ma et al., 2024c), driven by the scaling law demonstrating increased model parameters and training data with enhanced model performance. Unlike U-Nets, which apply convolutional layers capturing spatial hierarchies, DiTs segment the input into latent patches and leverage the transformer’s self-attention mechanism to model relationships within and across these patches.

In DiTs, the input noisy latent representation is decomposed into patches. These patches are embedded into tokens and fed into a series of DiT blocks. DiT blocks generally incorporate Multi-Head Self-Attention, Layer Norm, and Point-wise Feedforward Networks. However, the specifics of different DiT models may vary. For instance, the incorporation of conditioning can be achieved through various methods such as adaptive layer norm (Peebles & Xie, 2023), cross-attention (Chen et al., 2023), and extra input tokens (Esser et al., 2024). As diffusion models tackle higher-resolution images and longer visual sequences, they impose a quadratic computational burden on inference.

Input Temporal Redundancy: Diffusion Model entails the iterative prediction of noise from the input image or video. Recent research has highlighted the concept of *input temporal redundancy*, which refers to the similarity observed in both the inputs and activations across successive diffusion timesteps (So et al., 2023; Ma et al., 2024b). A recent study (Ma et al., 2024a) further investigates the distribution of this similarity across different layers and timesteps. Based on the redundancy, a branch of research caches the activation values and reuses them in the subsequent diffusion timesteps to prune computation. For example, in the context of the U-Net architecture, DeepCache updates the low-level features while reusing the high-level ones from cache (Ma et al., 2024b). Additionally, TGATE caches the cross-attention output once it converges along the diffusion process (Ma et al., 2024b). By contrast, in the domain of DiT models, Δ -DiT proposes to cache the rear DiT blocks in the early sampling stages and the front DiT blocks in the later stages (Chen et al., 2024b). PAB (Zhao et al., 2024) exploits the U-shaped attention pattern to mitigate temporal redundancy through a pyramid-style broadcasting approach. Finally, DiTFastAttn (Yuan et al., 2024) identifies three types of redundancies, such as spatial redundancy, temporal redundancy, and conditional redundancy, and presents an attention compression method to speed up generation.

Parallel Inference for Diffusion Model: Given the similar transformer architecture, tensor parallelism (TP) (Shoeybi et al., 2019) and sequence parallelism (SP) (Jacobs et al., 2023; Liu et al., 2023; Li et al., 2023), which are commonly employed for efficient inference in LLMs, can be adapted for DiTs. TP partitions model parameters across multiple devices, enabling parallel computation and reducing memory requirements on individual devices. However, it necessitates an AllReduce operation for the outputs of both the Attention and Feedforward Network modules, resulting in communication overhead proportional to sequence length. For DiTs with exceptionally long sequences, this communication overhead becomes substantial. In contrast, SP partitions the input image across multiple devices, utilizing methods such as Ulysses or Ring to communicate the Attention input and output tensors. SP demonstrates su-

perior communication efficiency compared to TP, but each device stores the entire model parameters, which can be memory intensive. DistriFusion (Li et al., 2024) leverages Input Temporal Redundancy to design an asynchronous sequence parallel method that utilizes stable activations. It is specifically designed for with a U-Net-based models.

3 METHODS

In this section, we delve into the application of tensor parallelism (TP), sequence parallelism (SP), and an asynchronous SP variant, namely DistriFusion, for parallel inference in DiTs. Following this, we introduce a novel patch-level pipeline parallel approach that markedly improves communication efficiency compared to existing techniques.

In the remaining of this article, the following notations are used: p denotes the sequence length, which corresponds to the number of pixels in the latent space. hs represents the hidden size of the model. L stands for the number of network layers. N is the number of computing devices.

3.1 Tensor Parallelism

When the DiT blocks consist of Multi-Head Self-Attention followed by a Feed-Forward Network (FFN), tensor parallelism (Shoeybi et al., 2019) (TP) can be applied to this architecture by parallelizing the linear layers in a column-wise manner after a row-wise manner. TP requires two all-reduce operations in both the attention and FFN layers, resulting in a communication overhead of $4O(p \times hs)$ for each layer, as shown in Table 1. This communication overhead is directly proportional to the sequence length, making it particularly significant for long sequences, where the communication cost becomes substantial. For instance, the 0.6B Pixart Model demonstrates poor scalability with Tensor Parallelism (TP), as illustrated in Figure 8. Moreover, for non-standard Transformer structures, such as the Multimodal(MM)-DiT blocks used in Flux and Stable Diffusion 3, arranging column-wise and row-wise weight partitioning presents substantial challenges. Consequently, we did not implement tensor parallelism for these structures.

3.2 Sequence Parallelism

In DiTs, 2D latent images can be flattened into visual token sequences, serving as inputs for transformer computation. Parallel computing along the sequence dimension involves partitioning the image into non-overlapping patches, with each device handling its local patch. The transformer’s attention mechanism (Vaswani et al., 2017) necessitates that each token attends to all others. However, each device only has $1/N$ of the Queries (Q), keys (K), and values (V), necessitating communication to gather intermediate results from other devices.

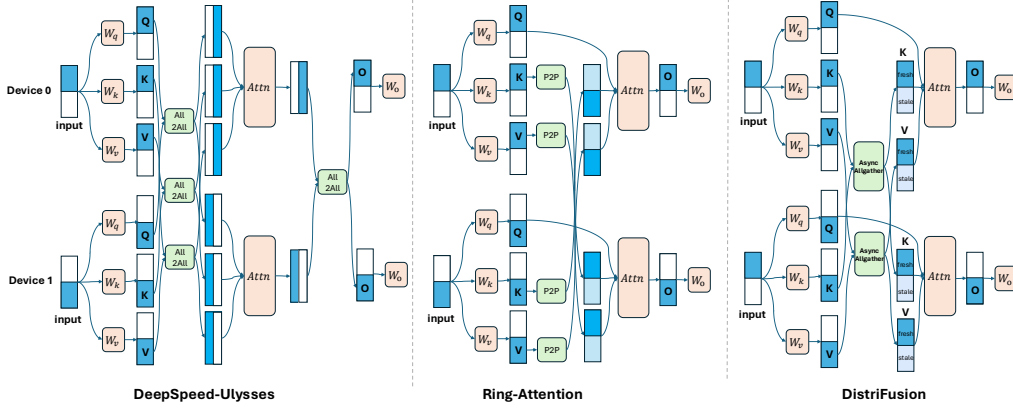


Figure 2. The DistriFusion vs. Sequence Parallelism of DeepSpeed-Ulysses (SP-Ulysses) and Ring-Attention (SP-Ring) for an Attention Module.

The current best practices for sequence parallelism are DeepSpeed-Ulysses (Jacobs et al., 2023) (SP-Ulysses), Ring Attention (Liu et al., 2023) (SP-Ring) or a hybrid of both (Fang & Zhao, 2024). As shown in Figure 2, SP-Ulysses employs All2All communications to transform the sequence dimension partitioning into partitioning along the hidden size, enabling parallel computation of attention across different heads. SP-Ring is a distributed version of Flash Attention, utilizing peer-to-peer (P2P) transmission of K and V subblocks. The outputs of sequence parallelism are consistent with those obtained from single device computation.

3.3 DistriFusion: Asynchronous Sequence Parallelism

DistriFusion is an asynchronous sequence parallelism technique that exploits input temporal redundancy, observed as high similarity in inputs and activations across successive diffusion timesteps (Li et al., 2024; Ma et al., 2024b). This redundancy allows the use of slightly outdated (stale) activations from the previous timestep instead of relying solely on fresh activations. Despite using stale activations, DistriFusion maintains image generation accuracy with no perceptible loss in quality to the human eye.

While DistriFusion was initially applied to U-Net-based SDXL models (Podell et al., 2023), it can be extended to DiT models as well. As illustrated in Figure 2, DistriFusion also operates by partitioning along the sequence dimension. The key distinction, however, lies in its use of asynchronous all-gather operations to collect K and V activations from remote devices. Due to the asynchronous nature of this communication, the activations for the current diffusion step are not immediately available; instead, they become accessible during the next diffusion step.

DistriFusion exploits this by utilizing a fraction $\frac{N-1}{N}$ of the K and V activations from timestep $T + 1$, combined with a

fraction $\frac{1}{N}$ of the local K and V from diffusion timestep T . This combination is used to compute the attention operation with the local queries at diffusion timestep T . The communication of K and V for timestep T is intentionally overlapped with the network’s forward computation at timestep T , thus hiding communication overhead during computation.

However, DistriFusion achieves this communication-computation overlap at the cost of increased memory usage. Each computational device is required to maintain communication buffers that store the complete spatial shape of the K and V activations, which amounts to AL in total. Consequently, the memory cost of DistriFusion does not scale down with the addition of computational devices.

3.4 PipeFusion: Patch-level Pipeline Parallel

Existing parallel paradigms, whether Tensor Parallel or Sequence Parallel, require communication of activations for each DiT’s block. The sequence-level pipeline parallel method proposed by TeraPipe (Li et al., 2021), used in LLMs, can transmit only limited input Activations, and has been proven to be more suitable for long sequence input (Qin et al., 2024). However, TeraPipe is designed for transformers using causal attention, where each token only attends to its previous tokens. In contrast, DiTs employ full attention, where each token attends to the computation of both previous and subsequent tokens. Nevertheless, by leveraging Input Temporal Redundancy, we found that TeraPipe can be perfectly applied to DiTs inference. We propose PipeFusion, a patch-level pipelined parallel approach for DiTs, which leverages the input temporal redundancy but exhibits enhanced communication and memory efficiency.

PipeFusion simultaneously partitions the input sequence and the layers of the DiTs backbone as shown at the top of Figure 3. PipeFusion partitions the DiTs model along the direction of data flow. Therefore, each partition contains a set of

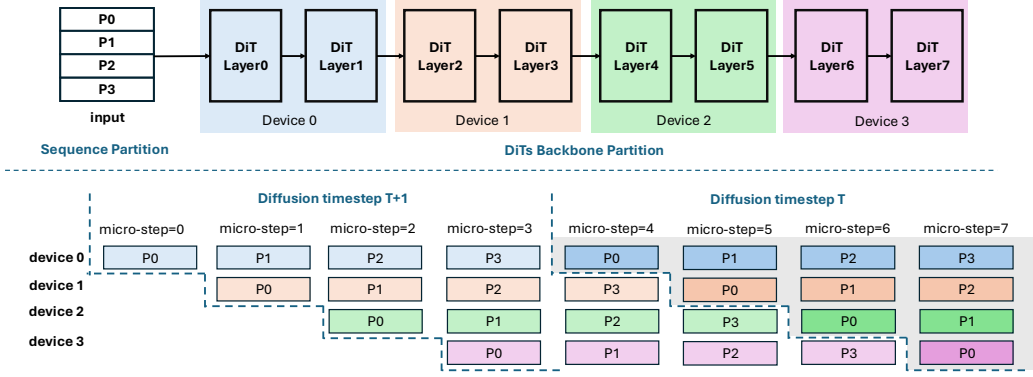


Figure 3. Above: partitioning strategy for Input and DiTs backbone network. Below: Workflow of the PipeFusion as patch-level pipelined parallelism.

consecutive layers and is deployed on a GPU. PipeFusion also partitions the input image into M non-overlapping patches so that each GPU processes the computation for one patch with its assigned layers in parallel, and the diffusion routine runs efficiently in a pipelined manner. Pipelining requires synchronizations between devices, which would be efficient if the DiT workload is evenly distributed across each GPU. The even partition is easy to achieve as a DiT contains numbers of identical transformer blocks.

Suppose we are currently at diffusion timestep T , the previous timestep is $T + 1$ as the diffusion process goes along the reversed order of timesteps. The example in Figure 3 demonstrates the pipeline workflow with $N = 4$ and $M = 4$, where the activation values of patches at timestep T are highlighted. Due to the input temporal redundancy, a device does not need to wait for the receiving of full spatial shape activations for the current timestep T to start the computation of its own stage. Instead, it employs the stale activations from the previous timestep to provide context for the current computation. For instance, in micro-step 5, the activations for Patches P0 and P1 are from timestep T , while others are from timestep $T + 1$. In this way, each device maintains the full activations and there is no waiting time after the pipeline is initialized. Bubbles only exist at the beginning of the pipeline. Suppose the total number of diffusion timesteps is S , then the effective computation ratio of the pipeline is $\frac{M \cdot S}{M \cdot S + N - 1}$. As S is commonly chosen to be large number for high-quality image generation, the effective computation ratio is high. For example, when $M = N = 4$ and $S = 50$, the ratio is equal to 98.5%.

Moreover, in PipeFusion, a device sends micro-step patch activations to the subsequent device via asynchronous P2P, enabling the overlap between communication and computation. For example, at micro-step 4, device 0 receives P1’s activation from diffusion timestep T while concurrently computing the activation values for P0 at timestep T . Similarly, at the next micro-step, the transmission of P0 to device

1 can be hidden by the computation of P1 on the device.

Similar to DistriFusion, before executing the pipeline, we usually conduct several diffusion iterations synchronously, called warmup steps. During the warmup phase, patches are processed sequentially, resulting in low efficiency. Though the warmup steps cannot be executed in the pipelined manner, the workflow is relatively small compare to the entire diffusion process, and thus, the impact on performance is negligible. We will analyze the impact of warmup and proposed the corresponding solutions in Sec. 6.

PipeFusion simultaneously partitions the image and the model layers to form a pipeline, which is also adopted by a previous method TeraPipe (Li et al., 2021). However, there are significant differences between the two methods. Firstly, TeraPipe is designed for training language models and leverages the properties of causal attention, where each token only attends to the attention computation of its previous tokens. In contrast, DiTs employ full attention, where each token attends to the computation of both previous and subsequent tokens. The full attention mechanism requires the usage of input temporal redundancy to construct pipelines. Secondly, TeraPipe adopts complex partition methods over the sequence dimension to achieve load balancing, which is not needed in PipeFusion.

3.5 Comparison Between Different Parallelisms

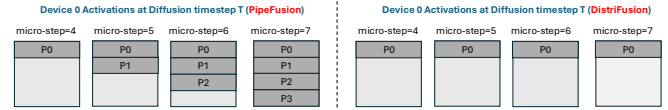


Figure 4. The fresh part of activations during diffusion timestep T of Figure 3. The dark gray represents fresh data and the light gray represents stable data.

Compared with existing parallel solutions, PipeFusion demonstrates superior efficiency in communication, mem-

Table 1. Comparison between different DiT parallel methods on a single diffusion timestep. Overlap denotes the overlapping between communication and computation.

Method	Communication		Memory Cost	
	Cost	Overlap	Model	KV Activations
Tensor Parallel	$4O(p \times hs)L$	✗	$\frac{1}{N}P$	$\frac{1}{N}KV$
DistriFusion	$2O(p \times hs)L$	✓	P	$(KV)L$
SP-Ring	$2O(p \times hs)L$	✓	P	$\frac{1}{N}KV$
SP-Ulysses	$\frac{4}{N}O(p \times hs)L$	✗	P	$\frac{1}{N}KV$
PipeFusion	$2O(p \times hs)$	✓	$\frac{1}{N}P$	$\frac{1}{N}(KV)L$

ory usage, and generation accuracy. Firstly, PipeFusion transmits between computational devices only the activations that serve as inputs and outputs for a series of consecutive transformer layers belonging to a stage, significantly reducing the communication bandwidth requirement in comparison to other methods that transmit the KV activations for all the L layers. In particular, the total communication cost for PipeFusion is $2O(p \times hs)$, not associating with the number of layers L . Secondly, each device in PipeFusion stores only $\frac{1}{N}$ of the parameters belonging to its specific layers. Since the usage of stale KV for attention computation requires each device to maintain the full spatial KV for the $\frac{L}{N}$ layers on the device, the overhead is significantly smaller than that of DistriFusion and diminishes as the number of devices increases. Thirdly, PipeFusion theoretically outperforms DistriFusion considering the area of fresh activation area. As shown in Figure 4, within a single diffusion timestep, PipeFusion continuously increases the area of fresh activation as the pipeline micro-steps progress from diffusion timestep 4 to 8. In contrast, throughout the entire diffusion process, DistriFusion constantly maintains one patch of fresh area out of the total M patches.

In the following, we summarize the theoretical cost of existing methods in Table 1. The communication cost is calculated by the product of the number of elements to transfer with an *algorithm bandwidth (algbw)* factor related to communication type ¹. For collective algorithms of AllReduce, AllGather and AllToAll, the corresponding algbw factors are $2\frac{n-1}{n}$, $\frac{n-1}{n}$, and 1. In the table, we approximate the term $O(\frac{n-1}{n})$ to $O(1)$ for simplicity.

Among all methods, PipeFusion has the lowest communication cost, as long as $N < 2L$, which is easy to satisfy as the number of network layers L is typically quite large, e.g., $L = 38$ in Stable-Diffusion-3. In addition, PipeFusion overlaps communication and computation. Ulysses Seq Parallel exhibits a decreasing communication cost with increasing N , outperforming the remaining three methods. However, its communication cannot be hidden by computation. Ring Seq Parallel and DistriFusion have similar communication

costs and overlapping behaviors. The distinction lies in the scope of overlapping: computation in Ring Seq Parallel overlaps within the attention module, whereas that in DistriFusion overlaps throughout the entire forward pass.

To analyze the memory costs, we denote P as the total number of model parameters. In PipeFusion and tensor parallelism, the memory cost decreases as more GPUs are utilized, which is a nice property with the rapid growth of the DiT model size. Both PipeFusion and DistriFusion maintain a KV buffer for each transformer layer leading to significant activation memory overhead, especially for long sequences. The KV buffer in PipeFusion decreases as the number of devices N increases, whereas DistriFusion does not exhibit such a reduction.

4 EXPERIMENTS

4.1 Setups

In our experimental setup, we deployed our trials on an $8 \times L40-48GB$ (PCIe Gen4x16) cluster to evaluate three prominent DiT models.

Pixart (Chen et al., 2023; 2024a): Its backbone is a transform model that encompasses 0.6B (billion) parameters. Pixart draws its architectural foundation from the original DiTs framework, with a pivotal enhancement: the integration of cross-attention modules designed to incorporate text conditions into the model’s processing.

Stable-Diffusion-3 (Esser et al., 2024) (SD3-medium): which leverages a Multimodal (MM)-DiT and its backbone transformer model contains 2B parameters. As the largest open-source variant available, SD3-medium employs a 20-step FlowMatchEulerDiscreteScheduler.

Flux.1-dev (BlackForestLabs, 2024): Its backbone transformer model contains 12B parameters and features an enhanced MM-DiT design. Flux.1-dev also relies on a 28-step FlowMatchEulerDiscreteScheduler.

4.2 Performance Results

This section compares the performance of different parallel methods on $8 \times L40$ GPUs, connected by PCIe Gen4. This section only presents the latency of the DiT except for the latency of the VAE decoding, since VAE module is the same across different parallel methods. Since the Pixart and SD3 can utilize Classifier-Free Guidance (CFG) (Ho & Salimans, 2022), we additionally implemented the CFG parallel. For an input prompt, CFG parallel individually computes the forward tasks for both unconditional guidance and text guidance. It leverages inter-image parallel to perform these two tasks, collecting the results after each diffusion step is completed. For PipeFusion, we select the best latency performance by searching the patch number M from 2, 4, 8,

¹<https://github.com/NVIDIA/nccl-tests/blob/master/doc/PERFORMANCE.md>

PipeFusion: Patch-level Pipeline Parallelism for Diffusion Transformers Inference

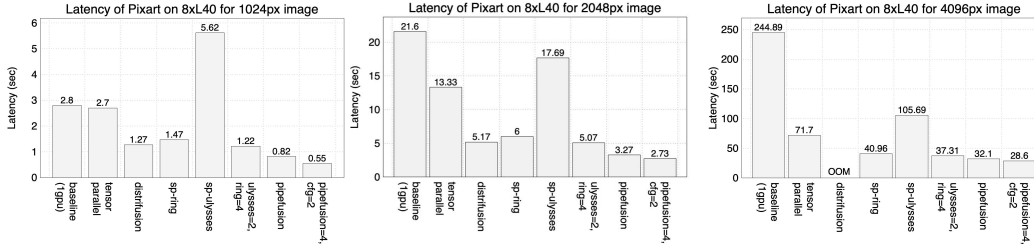


Figure 5. Latency on Pixart of various parallel approaches on two image generation tasks with the 20-Step DPMSolverMultistepScheduler.

16, 32. All figures show the average latency of 5 runs. We employ a default warmup step of 1 for both DistriFusion and PipeFusion. The software stack utilized includes PyTorch 2.4.1, CUDA Runtime 12.1.105, and diffusers 0.30.3.

4.2.1 Latency Evaluation

Pixart: Figure 5 shows the inference latency of Pixart on image generation tasks with resolution as 1024px (1024×1024), 2048px (2048×2048) and 4096px (4096×4096) on 8×L40.

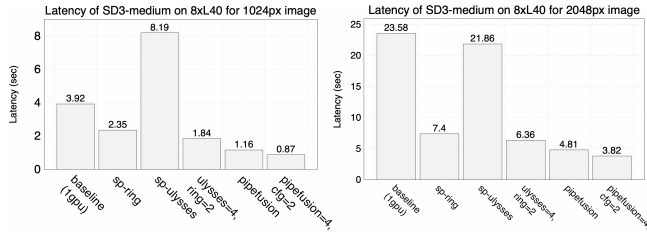


Figure 6. Latency on SD3-medium of various parallel approaches on two image generation tasks with the 20-Step FlowMatchEulerDiscrete Scheduler.

PipeFusion exhibits the lowest latency among parallel methods across all three tasks. **PipeFusion is 1.48×, 1.55×, and 1.16× faster than the second best parallel approaches on the 1024px, 2048px and 4096px tasks.**

The highest latency parallelism is always SP-Ulysses, primarily due to the bandwidth bottleneck between CPU sockets by conducting All2All on 8 GPUs via PCIe. SP-Ring exhibits significantly lower latency compared to SP-Ulysses. An efficiency method USP (Fang & Zhao, 2024) can further improve SP performance by hybridizing SP-Ulysses and SP-Ring. It views the process group as a 2D mesh where the columns are SP-Ring groups and the rows are SP-Ulysses groups. USP parallelizes the attention head dimension in SP-Ulysses groups and parallelizes the sequence dimension in SP-Ring groups. USP yields a lower latency than SP-Ring, as illustrated by the ulysses=2 and ring=4 columns in the figure.

Additionally, tensor parallel also shows high latency, which aligns with our analysis in section 3.5. DistriFusion exhibits

slightly higher latency compared to the USP (ulysses=2 and ring=4), and it encounters out-of-memory (OOM) issues on the 4096px task.

Using the CFG parallel, the 8 GPUs are divided into two groups, each performing PipeFusion independently, which can further reduce latency. This approach (cfg=2, pipefusion=4 in the figure) achieves a latency reduction of 5.09x, 7.91x, and 8.59x compared to the baseline (1 GPU). PipeFusion achieves perfect scalability in tasks 2048px and 4096px.

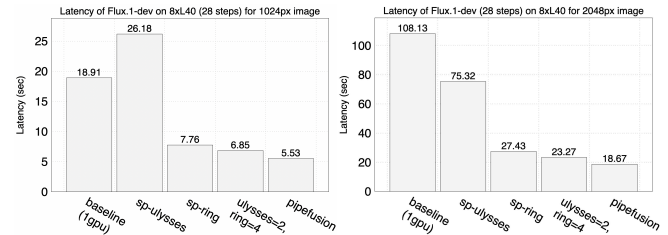


Figure 7. Latency on Flux.1-dev of various parallel approaches on three image generation tasks with the 28-Step FlowMatchEulerDiscrete Scheduler.

Stable Diffusion 3: Figure 6 shows the inference latency of SD3-medium on image generation tasks with resolution as 1024px, 2048px on 8×L40. The model is unable to generate 4096px images due to positional encoding limitations. Since MM-DiT applied in SD3 is a non-standard transformer layer, arranging column-wise and row-wise weight partitioning poses significant challenges, and we did not implement tensor parallelism. Additionally, due to potential OOM issues with DistriFusion and inferior performance compared with USP, we did not implement it for SD3.

PipeFusion outperforms the best sequence parallelism in these two cases, both of which are also the USP with ulysses=4, ring=2, **achieving speedups of 1.57× and 1.30×**. When combined with CFG parallel, the pipefusion=4, cfg=2 scheme on 8 GPUs achieves speedups of 3.11× and 8.16× compared to the baseline (1 GPU).

Flux.1-dev: Figure 7 illustrates the inference latency of SD3-medium on image generation tasks with resolutions

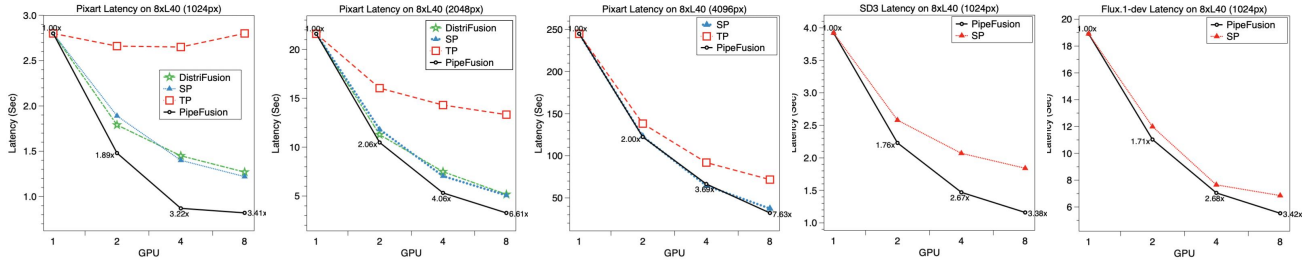


Figure 8. Scalability Analysis of Three DiTs on 8xL40: Leftmost figures depict Pixart performance on 1024px, 2048px, and 4096px images. The second from the right shows SD3 performance on 1024px. The rightmost figure illustrates Flux.1-dev performance on 1024px. The speedup to 1 GPU baseline is labeled on the points of pipefusion curves.

of 1024px and 2048px, respectively, using 8xL40. Flux.1 employs a similar MM-DiT architecture to SD3 but extends the network depth to 57 layers.

In both scenarios, PipeFusion surpasses the best sequence parallelism, which is also the USP with $ulysses=4$ and $ring=2$, achieving speedups of $1.23\times$ and $1.25\times$. PipeFusion offers $3.42\times$ and $5.79\times$ speedup compared to the baseline (1 GPU) for the two cases.

Scalability: We evaluated the scalability of inference for three models by scaling from 1 to 2, 4, and 8 GPUs. Figure 8 illustrates the scalability of different parallel approaches. PipeFusion and DistriFusion both apply a single warmup iteration. We applied USP to represent SP by searching for the optimal combination of $ulysses$ degree and $ring$ degree to achieve the best performance. The results show that PipeFusion consistently exhibits the best scalability across all five scenarios. Given that Pixart has the smallest model size, tensor parallelization unsurprisingly exhibits the worst scalability. Except for the Pixart 4096px case, PipeFusion significantly outperforms both SP and DistriFusion. In the Pixart 4096px scenario, PipeFusion and SP exhibit similar scalability, while DistriFusion encounters out-of-memory (OOM) issues and thus lacks corresponding data. This is likely due to the exceptionally long sequence, where the communication overhead becomes less significant, thereby diminishing the advantage of PipeFusion’s communication efficiency.

4.2.2 Memory Efficiency

We collect the memory usage excluding the VAE usage, which involves the computation of the text-encoder and DiTs backbones, as shown inAs shown in Figure 1. The figure includes memory usage for “parameters”, which encompasses both the text encoder and transformers, as well as for “activations”, which includes activations and temporary buffers. Note that SP-Ulysses, SP-Ring and USP exhibit similar memory consumption, denoted as SP in the figure.

The maximum memory usage of different parallel ap-

proaches for Pixart is depicted in Figure 9. The Pixart model consists of a 0.6B parameter DiT backbone (2.3 GB on disk) and T5-based text encoders (18GB on disk). So the memory consumption of parameters is dominated by the text encoder. DistriFusion maintains full spatial shape K, V tensors for each layer, resulting in an increase in memory consumption as the image resolutions grow. In contrast, PipeFusion only needs to store $1/N$ of the full spatial shape K, V tensors. Consequently, on 8xGPUs, its memory footprint is comparable to that of Tensor Parallel and Sequence Parallel. Remarkably, even for tasks with an 8192px resolution, PipeFusion exhibits the lowest memory consumption.

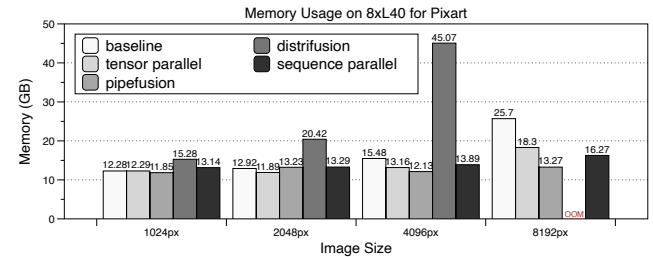


Figure 9. Max GPU Memory Usage of Various Approaches for Pixart Image Generation Tasks Across Four Resolutions.

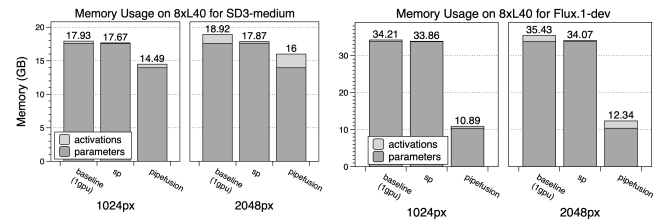
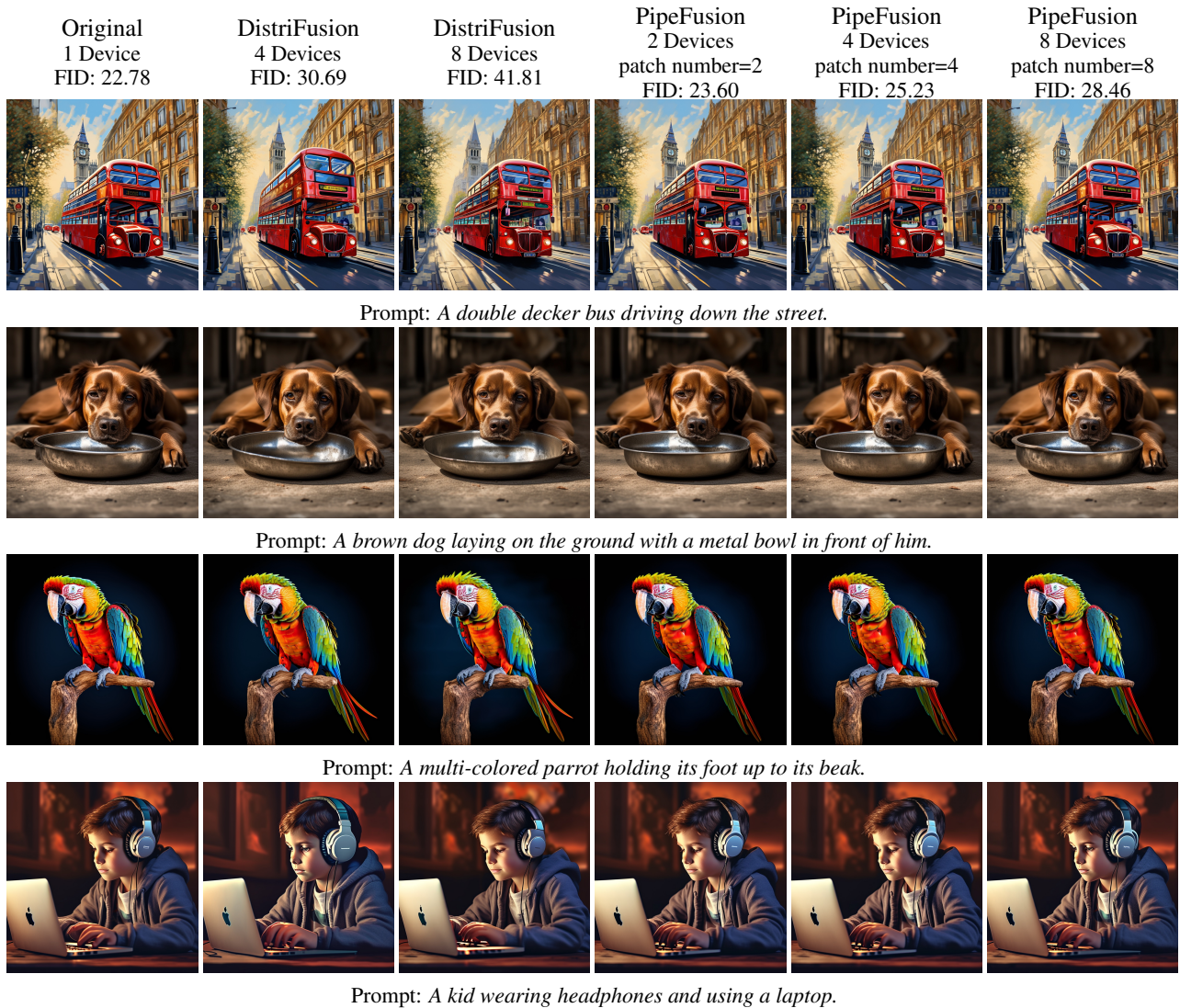


Figure 10. Max GPU Memory Usage on 8 GPUs for SD3-medium and Flux.1 on 1024px and 2048px image generation tasks.

The maximum memory usage of sequence parallel and PipeFusion for SD3-medium and Flux.1-dev is depicted in Figure 10. The SD3-medium consists of a 2B parameter DiTs backbone (7.8 GB on disk) and text encoders of nearly 19GB on disk. The Flux.1-dev consists of a 12B parame-



Model		PixArt-XL-2-256-MS						FLUX.1[dev]		
Method	Original	DistriFusion		PipeFusion			Original	PipeFusion		
Device Number	1	4	8	2	4	8	1	4	8	
FID ↓										
w/ G.T.	22.78	30.69	41.81	23.60	25.23	28.46	25.03	24.17	25.97	
w/ Orig.	-	8.41	19.81	1.67	3.11	6.09	-	4.01	5.93	

FID Scores for Parallel Methods on the Pixart and Flux.1. w/ G.T. means calculating the FID metrics with the ground-truth images. w/ Orig. means calculating the FID metrics with the images generated by the 1-Device original implementation.

Figure 11. Above: Showcases for 1024px Generation Images of PipeFusion and DistriFusion using Pixart. Bottom: FID Scores Evaluated for Pixart and Flux.1. We use a 20-step DPM-Solver with the warmup step set to 1 for DistriFusion and PipeFusion. We use the COCO Captions 2014 (Chen et al., 2015) dataset to evaluate the FID scores. During the evaluation, a subset comprising 30,000 images is sampled from the validation set and resized to 256px to serve as the reference dataset. Concurrently, each experiment generates 30,000 images of 256px, each paired with a caption derived from the COCO Captions 2014 dataset, as the sample dataset. The quality of images generated by PipeFusion closely resembles that of the original images, regardless of whether 4 or 8 devices are used, and across varying patch numbers. FID above the images is computed against the ground-truth images using Clean-FID (Parmar et al., 2022)

ter DiTs backbone (23 GB on disk) and text encoders of nearly 9.1GB on disk. The memory cost of PipeFusion is also significantly less than that of sequence parallelism. For the 12B Flux.1-dev, PipeFusion significantly reduces the memory footprint of model parameters. However, PipeFusion increases the memory usage of activations due to the consumption of the KV Buffer. Nevertheless, this increase is relatively minor compared to the overall model parameter memory usage. *The overall memory usage of PipeFusion is 32% and 36% of SP on 1024px and 2048px cases using Flux.1.*

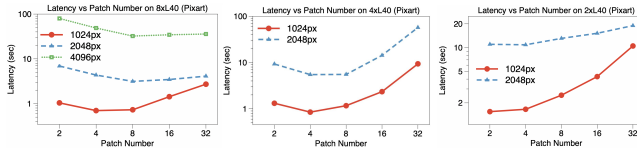


Figure 12. Latency of PipeFusion (without warmup) for various patch numbers M on 2x, 4x, and 8xL40 GPUs in image generation tasks at three different resolutions using Pixart.

5 QUALITY RESULTS

In Figure 11, we show visual results. The images generated by PipeFusion are nearly indistinguishable from the original images to the human eye, across various configurations of the number of patches and devices. The table at the bottom of the figure includes the Fréchet Inception Distance (FID) (Heusel et al., 2017), where a lower FID score is indicative of better performance, evaluated on Pixart and Flux.1. This data clearly indicates that *PipeFusion outperforms DistriFusion in terms of FID across the same device configurations*. This is because, compared to DistriFusion, PipeFusion utilizes more fresh KV values in its computations.

6 ABLATION STUDY

Patch Number: We analyze the impact of the setting of patch numbers M on PipeFusion as shown in Figure 12. According to the analysis presented in Table 1, M does not affect the communication cost. However, as shown in the figure, the lowest latency is achieved when M is equal to the number of GPUs, N . If M is large, the input size for operators becomes smaller, which can negatively impact the computational efficiency of the operator. In contrast, if M is small, the efficiency of overlapping communication and computation decreases.

Warmup Step: The number of warmup steps can negatively impact the overall performance of PipeFusion. The input temporal redundancy is relatively small during the initial few diffusion timesteps. Therefore, it is usually to employ a few warmup steps to enable synchronous communication

without resorting to stale activations, which would introduce waiting time, commonly referred to as bubbles, into the pipeline. As the number of sampling steps increases, the latency will also increase, as shown in Table 2. If the proportion of warmup steps is relatively small, no action is required. Our experiments involved a relatively small number of sampling steps, specifically 20 and 28. In other related work, it is common to use 50 steps (Li et al., 2024) or even 100 steps (Ma et al., 2024b), which helps to alleviate the overhead of warmup.

Warmup	pixart		sd3-medium		Flux.1-dev
	pp=8	cfg=2, pp=8	pp=8	cfg=2, pp=8	pp=8
0	0.71	0.66	1.05	0.83	5.48
1	0.82 (+15%)	0.69 (+4%)	1.16 (+10%)	0.87 (+4%)	5.53 (+1%)
2	0.91 (+28%)	0.7 (+6%)	1.27 (+21%)	0.92 (+11%)	6.00 (+9%)

Table 2. Impact of the warmup step number to Pixart, sd3-medium and Flux.1-dev on 1024px image generation, where pp indicates pipefusion (pp) parallel degree.

To mitigate the performance degradation caused by warmup, we can separate the warmup steps from the remaining working steps and allocate different computational resources to them. The output feature maps after the warmup steps can then be transmitted from the warmup devices to the working devices. The warmup phase can apply sequence parallelism to fully utilize the computational resources.

We found that the setting of warmup steps is highly dependent on the model. By initializing the KV buffer to zero and not performing warmup, Pixart can still achieve satisfactory image generation results. Through dynamic detection of the difference between the latent space input and the previous diffusion step, we can automatically set the warmup steps. These optimizations for warm-up will be our future work.

7 CONCLUSION

This paper introduces PipeFusion to parallelize Diffusion Transformers (DiTs) inference on multiple devices. By exploiting the input similarities across diffusion timesteps and employing a patch-level pipelined approach to orchestrate communication and computation, PipeFusion reduces both communication bandwidth and memory demands, making DiT inference more efficient on PCIe-connected devices. In the future, we plan to scale DiT inference to low-end multi-node GPU clusters, for example, PCIe inside a GPU node and Ethernet between nodes. We anticipate that PipeFusion will achieve even greater advantages in such environments.

REFERENCES

- BlackForestLabs. Announcing black forest labs. <https://blackforestlabs.ai/announcing-black-forest-labs/>, 2024. Accessed: [2024.10].
- Chen, J., Yu, J., Ge, C., Yao, L., Xie, E., Wu, Y., Wang, Z., Kwok, J., Luo, P., Lu, H., et al. Pixart- α : Fast training of diffusion transformer for photorealistic text-to-image synthesis. *arXiv preprint arXiv:2310.00426*, 2023.
- Chen, J., Ge, C., Xie, E., Wu, Y., Yao, L., Ren, X., Wang, Z., Luo, P., Lu, H., and Li, Z. Pixart- σ : Weak-to-strong training of diffusion transformer for 4k text-to-image generation. *arXiv preprint arXiv:2403.04692*, 2024a.
- Chen, P., Shen, M., Ye, P., Cao, J., Tu, C., Bouganis, C.-S., Zhao, Y., and Chen, T. δ -dit: A training-free acceleration method tailored for diffusion transformers. *arXiv preprint arXiv:2406.01125*, 2024b.
- Chen, X., Fang, H., Lin, T.-Y., Vedantam, R., Gupta, S., Dollár, P., and Zitnick, C. L. Microsoft coco captions: Data collection and evaluation server. *arXiv preprint arXiv:1504.00325*, 2015.
- Esser, P., Kulal, S., Blattmann, A., Entezari, R., Müller, J., Saini, H., Levi, Y., Lorenz, D., Sauer, A., Boesel, F., et al. Scaling rectified flow transformers for high-resolution image synthesis. In *Forty-first International Conference on Machine Learning*, 2024.
- Fang, J. and Zhao, S. A unified sequence parallelism approach for long context generative ai. *arXiv preprint arXiv:2405.07719*, 2024.
- Heusel, M., Ramsauer, H., Unterthiner, T., Nessler, B., and Hochreiter, S. Gans trained by a two time-scale update rule converge to a local nash equilibrium. *Advances in neural information processing systems*, 30, 2017.
- Ho, J. and Salimans, T. Classifier-free diffusion guidance. *arXiv preprint arXiv:2207.12598*, 2022.
- Jacobs, S. A., Tanaka, M., Zhang, C., Zhang, M., Song, L., Rajbhandari, S., and He, Y. Deepspeed ulysses: System optimizations for enabling training of extreme long sequence transformer models. *arXiv preprint arXiv:2309.14509*, 2023.
- Jiang, Z., Lin, H., Zhong, Y., Huang, Q., Chen, Y., Zhang, Z., Peng, Y., Li, X., Xie, C., Nong, S., et al. Megascala: Scaling large language model training to more than 10,000 gpus. *arXiv preprint arXiv:2402.15627*, 2024.
- Kingma, D. P. and Welling, M. Auto-encoding variational bayes. *arXiv preprint arXiv:1312.6114*, 2013.
- Li, D., Shao, R., Xie, A., Xing, E. P., Gonzalez, J. E., Stoica, I., Ma, X., and Zhang, H. Lightseq: Sequence level parallelism for distributed training of long context transformers. *arXiv preprint arXiv:2310.03294*, 2023.
- Li, M., Cai, T., Cao, J., Zhang, Q., Cai, H., Bai, J., Jia, Y., Liu, M.-Y., Li, K., and Han, S. Distrifusion: Distributed parallel inference for high-resolution diffusion models. In *Proceedings of the IEEE/CVF Conference on Computer Vision and Pattern Recognition (CVPR)*, 2024.
- Li, Z., Zhuang, S., Guo, S., Zhuo, D., Zhang, H., Song, D., and Stoica, I. Terapipe: Token-level pipeline parallelism for training large-scale language models. In *International Conference on Machine Learning*, pp. 6543–6552. PMLR, 2021.
- Liu, H., Zaharia, M., and Abbeel, P. Ring attention with blockwise transformers for near-infinite context. *arXiv preprint arXiv:2310.01889*, 2023.
- Lu, C., Zhou, Y., Bao, F., Chen, J., Li, C., and Zhu, J. Dpm-solver: A fast ode solver for diffusion probabilistic model sampling in around 10 steps. *Advances in Neural Information Processing Systems*, 35:5775–5787, 2022.
- Ma, X., Fang, G., Mi, M. B., and Wang, X. Learning-to-cache: Accelerating diffusion transformer via layer caching. *arXiv preprint arXiv:2406.01733*, 2024a.
- Ma, X., Fang, G., and Wang, X. Deepcache: Accelerating diffusion models for free. In *Proceedings of the IEEE/CVF Conference on Computer Vision and Pattern Recognition*, pp. 15762–15772, 2024b.
- Ma, X., Wang, Y., Jia, G., Chen, X., Liu, Z., Li, Y.-F., Chen, C., and Qiao, Y. Latte: Latent diffusion transformer for video generation. *arXiv preprint arXiv:2401.03048*, 2024c.
- MetaAI. Movie gen: A cast of media foundation models. <https://ai.meta.com/static-resource/movie-gen-research-paper>, 2024. Accessed: 2024-10-14.
- OpenAI. Video generation models as world simulators. <https://openai.com/index/video-generation-models-as-world-simulators/>, 2024. Accessed: May 2024.
- Parmar, G., Zhang, R., and Zhu, J.-Y. On aliased resizing and surprising subtleties in gan evaluation. In *Proceedings of the IEEE/CVF Conference on Computer Vision and Pattern Recognition*, pp. 11410–11420, 2022.
- Peebles, W. and Xie, S. Scalable diffusion models with transformers. In *Proceedings of the IEEE/CVF International Conference on Computer Vision*, pp. 4195–4205, 2023.

- Podell, D., English, Z., Lacey, K., Blattmann, A., Dockhorn, T., Müller, J., Penna, J., and Rombach, R. Sdxl: Improving latent diffusion models for high-resolution image synthesis. *arXiv preprint arXiv:2307.01952*, 2023.
- Qin, R., Li, Z., He, W., Zhang, M., Wu, Y., Zheng, W., and Xu, X. Mooncake: Kimi’s kvcache-centric architecture for llm serving. *arXiv preprint arXiv:2407.00079*, 2024.
- Ronneberger, O., Fischer, P., and Brox, T. U-net: Convolutional networks for biomedical image segmentation. In *Medical image computing and computer-assisted intervention—MICCAI 2015: 18th international conference, Munich, Germany, October 5-9, 2015, proceedings, part III 18*, pp. 234–241. Springer, 2015.
- Shoeybi, M., Patwary, M., Puri, R., LeGresley, P., Casper, J., and Catanzaro, B. Megatron-lm: Training multi-billion parameter language models using model parallelism. *arXiv preprint arXiv:1909.08053*, 2019.
- So, J., Lee, J., and Park, E. Fdiff: Feature reuse for exquisite zero-shot acceleration of diffusion models. *CoRR*, abs/2312.03517, 2023. doi: 10.48550/ARXIV.2312.03517. URL <https://doi.org/10.48550/arXiv.2312.03517>.
- Song, J., Meng, C., and Ermon, S. Denoising diffusion implicit models. *arXiv preprint arXiv:2010.02502*, 2020.
- Vaswani, A., Shazeer, N., Parmar, N., Uszkoreit, J., Jones, L., Gomez, A. N., Kaiser, Ł., and Polosukhin, I. Attention is all you need. *Advances in neural information processing systems*, 30, 2017.
- Yuan, Z., Lu, P., Zhang, H., Ning, X., Zhang, L., Zhao, T., Yan, S., Dai, G., and Wang, Y. Ditfastattn: Attention compression for diffusion transformer models. *arXiv preprint arXiv:2406.08552*, 2024.
- Zhao, X., Jin, X., Wang, K., and You, Y. Real-time video generation with pyramid attention broadcast. *arXiv preprint arXiv:2408.12588*, 2024.